

Energy-Efficient Multidimensional Constellation Based on Leech Lattice for Visible Light Communications

Jia-Ning Guo, Ru-Han Chen*, Jian Zhang, Longguang Li, and Jing Zhou

Abstract—In this paper, a 24-dimensional geometrically-shaped constellation design based on Leech lattice is presented for indoor visible light communications (VLCs) with a peak- and an average-intensity input constraints. Firstly, by leveraging tools from large deviation theory, we characterize second-order asymptotics of the optimal constellation shaping region under aforementioned intensity constraints, which further refine our previous results in [Chen. et. al, 2020]. Within the optimal geometrical shaping region, we develop an energy-efficient 24-dimensional constellation design, where a significant coding gain brought by the Leech lattice and the nearly-maximum shaping gain are incorporated by using a strategy called coarsely shaping and finely coding. Fast algorithms for constellation mapping and demodulation are presented as well. Numerical results verifies the superiority of our results as compared with existing methods.

Index Terms—Visible light communication (VLC), single-input single-output (SISO), multidimensional constellations, constellation shaping, Leech lattice.

I. INTRODUCTION

As a potential candidate for the next-generation wireless communication technology, visible light communication (VLC) has gained significant attention owing to integrated usage of communication and illumination, license-free deployment, inherent security, and absence of electromagnetic interference. Especially for less complexity and lower cost, intensity modulation and direct detection (IM/DD) are widely used in the VLC [1]–[3]. In the IM/DD system, the information is modulated on the optical intensity emitted from light emitting diodes (LEDs) and recovered at the photodetector (PD) by measuring the intensity of the incoming light. For this reason, the intensity-modulated signal is required to be real and nonnegative, which is fundamentally distinguished from that in radio-frequency communication. Moreover, a peak- and/or an average-intensity constraint may be imposed on the channel input due to safety consideration, hardware limitation, and illumination requirement.

Conventionally, linear IM/DD optical wireless communication is modelled by the optical intensity channel (OIC),

where the effect of strong background radiation and thermal noise at PDs is assumed to be additive white Gaussian noise (AWGN) [4]–[6]. In recent years, extensive research has been conducted to characterize the capacity of various OICs under different intensity constraints or equipped with multiple transmitters and receivers, which lay a theoretical foundation of signaling designs for practical VLC systems [7]–[11]. Because of the short propagation distances, predominantly line-of-sight (LOS) environments, and relatively narrow modulation bandwidth of the LED device, indoor VLC systems usually operates at a high signal-to-noise ratio (SNR) condition [12], [13]. Therefore, it is necessary to investigate the capacity-approaching signaling design of the OIC at high SNRs. In [14], a space-time constellation design is provided for the multi-input single-output (MISO) VLC systems with a peak-intensity constraint. An average-intensity efficient constellation design for the MISO-VLC is proposed in [15]. In [16], [17], the 2-dimensional continuous-time signal space and constellation designs are developed for the bandlimited OIC. Constellation shaping is widely acknowledged as to be necessary to approach channel capacity in a high-SNR regime [18]. In traditional radio-frequency communications modelled as an AWGN channel under a quadratical constraint, the ultimate shaping gain is up to 1.53 dB with respect to the traditional SNR definition, while that of the OIC under an average-intensity constraint is 1.33 dB with respect to a modified SNR definition given in Sec. II [25]. Commonly-used shaping methods include the probabilistic shaping and the geometric shaping. The former one may not be suitable for the high-SNR case due to the need of distribution matching for a input set with a large cardinality [8]. In fact, a classic coded modulation scheme, called *lattice codes*, is widely used for bandlimited channels, which can be naturally combined with geometric shaping by the intersection of a densely-packed lattice (or its translate) and a well-chosen region in Euclidean space. In [19], for the OIC under a peak- and an average-intensity constraints, we investigated the optimal geometrical shaping problem and developed a geometrically shaped constellation based on the checkerboard lattice. However, there is no closed-form expression and a systematic understanding of the optimal shaping parameter, which is numerically computed in [19]. Additionally, another need for a finite-blocklength analysis of the constellation shaping theory for the OIC arises from the fact that significant coding gains and shaping gains can be attained in relatively short blocklengths by lattice codes [20], [21]. To overcome this disadvantage and further narrow the

This work is supported by the National Natural Science Foundation of China under Grant No. 62071489. Jia-Ning Guo and Jian Zhang are with National Digital Switching System Engineering and Technological Research Center, Henan Province (450000), China (e-mail: 14291003@bjtu.edu.cn, zhang_xinda@126.com). Ru-Han Chen is with Sixty-Third Research Institute, National University of Defense Technology, Nanjing, China (e-mail: tx_rhc22@nudt.edu.cn). Longguang Li is with Dept. Communication and Electronic Engineering, East China Normal University, Shanghai, China (e-mail: lgli@cee.ecnu.edu.cn). Jing Zhou is with Shaoxing University, Shaoxing, China (e-mail: jzee@ustc.edu.cn). (Corresponding Author: Ru-Han Chen.)

obvious gap between the existing signaling scheme and the fundamental limit, in this paper, we are devoted to designing an energy-efficient multidimensional lattice code for the indoor VLC under a peak- and an average-intensity constraints. The main challenges in multidimensional constellation design come from two aspects:

- 1) *Geometrical Shaping*: Unlike the AWGN channel with only a quadratic constraint, the presence of amplitude limitation usually leads to an irregular boundary of the optimal shaping region, and hence, hinders involved parameter selection and performance analysis in finite dimensions [22]. The main challenge in the geometrical shaping is to derive the optimal shaping parameter and accomplish the corresponding performance analysis for finite-dimensional cases in a more tractable form.
- 2) *Coded Modulation Design*: To further enhance the error performance, a more densely packing structure of constellation points should be utilized. However, how to efficiently incorporate the nearly-maximum shaping gain brought by an irregular region and a large coding gain by a densely-packed lattice in a coded modulation scheme is challenging.

In this paper, for the OIC with a peak- and an average-intensity constraints, we further improve previous results on the optimal shaping region and propose a 24-dimensional constellation design that incorporates the nearly-maximum shaping gain and a significant coding gain. The main contributions are summarized as follows:

- 1) *Closed-Form Approximation for Optimal Shaping Region*: To avoid numerical calculation involved in existing geometrically shaping methods, based on large deviation theory we characterize the second-order asymptotic behavior (as the blocklength tends to infinity) of the optimal shaping region, and a closed-form approximation for maximum shaping gains and shaping parameters is therefore given. Numerical simulation reveals a good match of our proposed approximation even at low dimensions.
- 2) *Optimally-Shaped Leech Constellation*: By exploiting the algebraic structure of the Leech lattice and the Leech half-lattice, we construct a 24-dimensional constellation, called *optimally-shaped Leech constellation*, that incorporates the nearly-maximum shaping gain and a larger coding gain by coarsely shaping in some sublattice and finely coding in Leech lattice. As compared to the cubic constellation, Nominal minimum Euclidean distance gain of 3-4.1 dB can be achieved by our proposed constellation design.
- 3) *Fast Algorithms for Constellation Mapping and Demodulation*: To efficiently and uniquely map binary data onto the irregularly bounded constellation with an exponentially increased cardinality, we explore the algebraic properties of the Leech lattice and decompose it into coarsely shaping lattice, Golay code and coset representative, mapping the binary data onto them respectively. At the receiver, we demodulate the constellation points by finding the closest point of the construction-

A lattice that is the union of Leech half-lattice and its cosets. The design can be realized with a relatively low implementation complexity by the algorithms.

The remainder of this paper is organized as follows. The channel model presented in Section II. In Section III, we review the optimal shaping region for optical intensity channel under dual intensity constraints and then characterize its second-order asymptotic properties. In Section IV, an optimally-shaped Leech constellation design is presented. Simulation results verify our results in Section V. Section VI concludes the whole paper.

II. CHANNEL MODEL

In this paper, we consider a single-input and single-output (SISO) VLC link whose channel output over n successive channel uses can be modeled by

$$\mathbf{r} = \mathbf{x} + \mathbf{z}, \quad (1)$$

where the n -dimensional real vector $\mathbf{x} = (x_1, \dots, x_n)$ denotes the instantaneously transmitted intensity signal equiprobably chosen from some multidimensional constellation \mathcal{X} , and the n -dimensional vector \mathbf{z} denotes the channel noise that modeled as the additive white Gaussian noise (AWGN) with zero mean and variance σ^2 [6].

Because the indoor visible light communication operates in the high-SNR regime [23] (also numerically verified in Section V), in this paper we mainly concern with multidimensional constellation design for intensity-modulated signals. Denote the cardinality of the constellation \mathcal{X} to be designed by $M \in \mathbb{N}_+$. Then the normalized bit rate of the constellation \mathcal{X} is $\beta = \frac{1}{n} \log_2 M$. Because of nonnegativity of intensity-modulated signals, the constellation \mathcal{X} is required to satisfy

$$\mathcal{X} \subseteq \mathbb{R}_+^n,$$

where the set \mathbb{R}_+^n denotes the nonnegative orthant consisting of all nonnegative vectors in Euclidean n -space. Moreover, for the reasons of illumination control, device limitation and safety requirement in VLCs, a peak- and an average-intensity constraints are imposed on the constellation \mathcal{X} as well¹

$$\max_{\mathbf{x} \in \mathcal{X}} \|\mathbf{x}\|_\infty \leq 1, \quad (2a)$$

$$\frac{1}{M} \sum_{\mathbf{x} \in \mathcal{X}} \sum_{i=1}^n x_i \leq \alpha; \quad (2b)$$

where the constant $\alpha \in (0, \frac{1}{2})$ denotes the ratio of the maximum allowed average intensity to the maximum allowed peak intensity.

For invariance to scaling, in this paper we define the SNR as the ratio of the maximum allowed peak intensity of the input signal to the standard deviation σ of the noise, i.e.,

$$\text{SNR} \triangleq \frac{1}{\sigma}. \quad (3)$$

¹Without loss of generality, the maximum allowed peak intensity and the channel coefficient in the SISO channel (1) can be simultaneously normalized to unity by scaling the noise variance σ^2 .

The main figure of merit of high-dimensional constellation is the minimum Euclidean distance (MED), which is given as follows

$$\min_{\substack{\mathbf{x}_1, \mathbf{x}_2 \in \mathcal{X} \\ \mathbf{x}_1 \neq \mathbf{x}_2}} \|\mathbf{x}_1 - \mathbf{x}_2\|_2. \quad (4)$$

With perfect channel state information (CSI) at the receiver, the error performance of the indoor VLC system at the high-SNR condition is primarily determined by the MED of the constellation \mathcal{X} . Therefore, the primary objective of our scheme is to design a constellation with the cardinality M that maximizes the MED.

III. OPTIMAL SHAPING REGION AND FINITE-BLOCKLENGTH ANALYSIS

Before presenting the optimal shaping region, it is necessary to clarify the duality between the one-dimensional maximum entropy distribution and the high-dimensional uniform distribution. Since the characteristics of the high-dimensional uniform distribution are determined by the geometric characteristics of the support set, it can also be considered as a geometric statement of the maximum entropy distribution.

In the next subsection, we will review the optimal choice of the region enclosing the lattice points for our considered channel.

A. Optimal Shaping Region

For self-containment of the paper, we first introduce the definition of *shaping gain* and then review our previous result on the optimal geometrically shaping region for optical intensity channels with both intensity constraints [19].

Denote the shaping region of the n -dimensional intensity-modulated constellation of \mathcal{X} by \mathcal{R} . Due to the peak-intensity constraint, it is required that $\mathcal{R} \subseteq [0, 1]^n$. In line with [14], [24], the baseline shaping region is given as the one-dimensional line segment $\mathcal{L}^\dagger = [0, 2\alpha]$. In the high-SNR regime, we utilize the n -dimensional uniform distribution $\mathbf{W}_n \sim \text{Unif}(\mathcal{R})$ and one-dimensional uniform distribution $W^\dagger \sim \text{Unif}(\mathcal{L}^\dagger)$ as the channel inputs respectively. Then the difference in their achievable rates can be approximated by

$$\begin{aligned} & \frac{1}{n} \mathbb{I}(\mathbf{W}_n; \mathbf{W}_n + \mathbf{Z}) - \mathbb{I}(W^\dagger; W^\dagger + Z) \\ & \approx \frac{1}{n} \log(\text{vol}(\mathcal{R})) - \log(2\alpha), \end{aligned} \quad (5)$$

where $\text{vol}(\mathcal{R})$ is the n -dimensional volume of \mathcal{R} . Due to the logarithm growth of the achievable rates for AWGN channels, we define the shaping gain as

$$\text{SG}(\mathcal{R}) \triangleq \exp\left(\frac{1}{n} \log(\text{vol}(\mathcal{R})) - \log(2\alpha)\right) = \frac{\sqrt[n]{\text{vol}(\mathcal{R})}}{2\alpha}, \quad (6)$$

which is also compatible with other definitions in [19], [24], [25].

For the input signal under a peak and an average-intensity constraints (2), finding the optimal shaping region in n -space can be formulated as the following problem

$$\begin{aligned} & \max \quad \frac{\text{vol}(\mathcal{R})^{1/n}}{2\alpha} \\ & \text{s.t.} \quad \mathcal{R} \subseteq [0, 1]^n \\ & \quad \int_{\mathcal{R}} \frac{\sum_{i=1}^n x_i}{\text{vol}(\mathcal{R})} dx_1 \cdots dx_n \leq n\alpha. \end{aligned} \quad (7)$$

In [19], the optimal shaping region for our considered OIC has been proved to be the family of truncated cubes (see Appendix A for details), and the setting of the parameter is given in the following theorem.

Theorem 1. (*Optimal Shaping [19]*) *The optimal solution to the problem (7) is $\mathcal{T}_n(t_n^*)$ as defined in Eq. (33), where the parameter t_n^* is determined by*

$$t_n^* = \begin{cases} P_n^{-1}(\alpha) & , \text{ if } \frac{1}{n+1} \leq \alpha < \frac{1}{2}, \\ (n+1)\alpha & , \text{ if } \alpha \leq \frac{1}{n+1}, \end{cases} \quad (8)$$

and $P_n(\cdot)$ is given in Eq. (35). Accordingly, the maximum shaping gain in Euclidean- n space is given by

$$\bar{\gamma}_\alpha(n) = \text{SG}(\mathcal{T}_n(t_n^*)) = \sqrt[n]{V_n(t_n^*)}/2\alpha. \quad (9)$$

We would like to point out that in Theorem 1 the parameter t_n^* is determined by the inverse of the average first moment $P_n(\cdot)$ that is strictly increasing. Although the bisection algorithm is applicable for solving (8), as the blocklength increases, the numerical method may become impractical due to the presence of factorials and polynomials in (34) and (35). Additionally, lack of closed-form expression or evaluation for the optimal shaping parameter t_n^* and the maximum shaping gain $\bar{\gamma}_\alpha(n)$ limits further analysis of properties of optimal shaping regions. To overcome this limitation, an asymptotic analysis of optimal shaping regions based on the large deviation theory is carried out in the subsequent subsection.

B. Finite-Blocklength Analysis of Optimal Shaping Region

Without loss of generality, we let $\tau = t/n$ and accordingly $\tau_n^* = t_n^*/n$. By leveraging tools from the large deviation theory (see Appendix B), we establish the asymptotic of τ_n^* in what follows.

Theorem 2. *For any given $\alpha \in (0, \frac{1}{2})$, the optimal shaping region satisfies*

$$\tau_n^* = \alpha + \frac{1}{\mu^*} \frac{1}{n} + o\left(\frac{1}{n}\right), \quad (10)$$

where μ^* is the unique positive solution to the following equation

$$\alpha = \frac{1}{\mu^*} - \frac{1}{\exp(\mu^*) - 1}. \quad (11)$$

Proof: See Appendix C. ■

Theorem 2 shows that the optimal shaping parameter τ_n^* converges to α at a rate of $\frac{1}{\mu^*} \frac{1}{n}$, where μ^* is also the

exponential decay rate of the following probability density function

$$p_X^*(x) = \frac{\mu^*}{1 - \exp(-\mu^*)} \exp(-\mu^*x), \quad 0 \leq x \leq 1, \quad (12)$$

that maximizes the differential entropy of the input X under the support constraint $X \in [0, 1]$ and the average-intensity constraint $\mathbb{E}[X] = \alpha$ [7].

Relying on Theorem 2, a second-order expansion of the maximum shaping gain can be obtained as follows.

Theorem 3. (Second-Order Approximation) *For any given $\alpha \in (0, \frac{1}{2})$, the maximum shaping gain $\bar{\gamma}_\alpha(n)$ achieved in the Euclidean- n space satisfies*

$$\log \bar{\gamma}_\alpha(n) = \mathbf{h}_{\max}(\alpha) - \log(2\alpha) - \frac{\log(n)}{2n} + \frac{\omega_\alpha}{n} + o\left(\frac{1}{n}\right) \quad (13)$$

where $\mathbf{h}_{\max}(\alpha)$ is the differential entropy of $p_X^*(x)$ in Eq. (12), and the constant ω_α is given by

$$\omega_\alpha = 1 - \frac{1}{2} \log\left(2\pi\left(-\mu^* + 2\alpha\mu^* + (\mu^*)^2\alpha(1-\alpha)\right)\right). \quad (14)$$

Proof: See Appendix D. ■

Theorem 3 demonstrates an interesting connection between the maximum-entropy distribution and the optimal shaping region for our considered channel, which reveals the superiority of the geometrical shaping at high-SNRs as the dimension increases.

In the following, such the connection will be further clarified. Define $\mathbf{X} = (X_1, \dots, X_n)$ as a random vector uniformly distributed on $\mathcal{T}_n(t_n^*)$. Due to the permutation-invariance property of $\mathcal{T}_n(t_n^*)$, we can investigate the marginal probability density function of the random variable X_1 , which is denoted by $f_{X_1,n}(x)$ for $x \in [0, 1]$. A convergence property of the marginal distribution of the optimal shaping region is given in Proposition 4.

Proposition 4. *As $n \rightarrow +\infty$, any marginal distribution of the random vector uniformly distributed on $\mathcal{T}_n(t_n^*)$ follows the maximum-entropy distribution (12), i.e.,*

$$f_\infty(x) = \lim_{n \rightarrow \infty} f_{X_1,n}(x) = p_X^*(x), \quad (15)$$

Proof: See Appendix E. ■

IV. OPTIMALLY-SHAPED LEECH CONSTELLATION

In Section III, we derive a closed-form expression for the optimal shaping parameter t_n^* and the corresponding maximized shaping gain $\bar{\gamma}_\alpha(n)$, which strengthen the result of geometrical constellation shaping given in [19]. In order to improve the coding gain, one approach is to employ an inequippable amplitude shift keying (ASK) constellation in conjunction with powerful channel codes like LDPC codes. However, it may not be suitable for indoor VLC scenarios due to the need of distribution matching and time-consuming iterative decoding algorithms. Therefore, in this section we focus on multidimensional constellation design, of which flexible transmission rates and substantial SNR gains consisting both

of shaping gains brought by geometrically shaping regions and coding gains by densely-packing lattices could be realized at the cost of relatively low implementation complexity.

Before a formal introduction of the design in this paper, we shall review truncated cubic constellations (TCCs) based on the checkerboard lattice D_n proposed in [19]. Some essential definitions are needed for subsequent statements and given in what follows.

The checkerboard lattice D_n is the sublattice of \mathbb{Z}^n that consists of all points with even sum, i.e.,

$$D_n = \{(x_1, \dots, x_n) \in \mathbb{Z}^n : x_1 + \dots + x_n \text{ is even}\}.$$

Let H and L be two nonnegative integers. Then we define the n -dimensional discrete cube with the parameter H as

$$\mathcal{C}_n(H) \triangleq \{0, 1, \dots, H\}^n,$$

and the D_n -based cube with the parameter H as

$$\mathcal{DC}_n(H) \triangleq D_n \cap \mathcal{C}_n(H), \quad (16)$$

i.e., the set of D_n points in $\mathcal{C}_n(H)$. The D_n -based truncated cube $\mathcal{D}_n(H, 2L)$ is defined as a subset of $\mathcal{DC}_n(H)$ which consists of all points with the ℓ_1 -norm no larger than $2L$, i.e.,

$$\mathcal{D}_n(H, 2L) \triangleq \left\{ \mathbf{x} \in \mathcal{DC}_n(H) \left| \sum_{i=1}^n x_i = 0, 2, \dots, 2L \right. \right\}. \quad (17)$$

A size- M TCC $\mathcal{D}_n(H^*, 2L^*, M)$ is a subset of a D_n -based truncated cube $\mathcal{D}_n(H^*, 2L^*)$, from which M points with least ℓ_1 -norm are selected. The parameters H^* and L^* are obtained by truncating the D_n lattice in the nearly-optimal shaping region, and can be readily computed by using Algorithm 1 in [19]. Moreover, an FFT/IFFT-based algorithm, say *FFT-assisted decomposable shell mapping* (FDSM), proposed in [19] can quickly enumerate points \mathbf{d} from a D_n -based truncated cube in the ascending order with respect to the ℓ_1 -norm of \mathbf{d} (in other word, the instantaneous intensity of \mathbf{d}), and hence, is used to map the message onto the TCC $\mathcal{D}_n(H^*, 2L^*, M)$. The D_n -based truncated cube as well as this fast mapping algorithm will also play an important role in our constellation mapping scheme.

A. Leech Lattice Construction

Clearly, both the shaping and the coding of TCCs are carried out by the checkerboard lattice D_n , of which a nominal coding gain of 1.5 dB (with respect to the SNR definition (3)) is attained as compared with the ASK constellation. In our design, we exploit the good algebraic structure of the Leech lattice Λ_{24} to argument the coding gain. The Leech lattice Λ_{24} is first introduced by J. Leech in [26], and recently proved to be the densest packing in 24-dimensional Euclidean space [27]. By using Leech lattice, an extra nominal coding gain of 3 dB (effective coding gain of 2 dB) may be attained. In the following, a brief introduction of construction of Leech lattice is given.

To facilitate constellation mapping, in this paper we construct the Leech lattice Λ_{24} based on the Leech half-lattice H_{24} with the following construction-C form [28], [29]:

$$H_{24} \triangleq 4\mathbb{Z}^{24} + 2C_{24} + G_{24} = 2D_{24} + G_{24}, \quad (18)$$

where C_{24} is the 24-dimensional parity check codes, G_{24} is the (24, 12, 8) Golay codes, and D_{24} denotes the 24-dimensional checkerboard lattice. Then the Leech lattice Λ_{24} can be constructed by

$$\Lambda_{24} = 2H_{24} \cup (2H_{24} + \xi), \quad (19)$$

where the 24-dimensional translation vector $\xi = (-3, 1^{23}) \in \mathbb{R}^{24}$ [30].

B. Optimally-Shaped Leech Constellation

To integrate the coding gain of Λ_{24} and the nearly-maximum shaping gain, a natural way to design multidimensional constellation is selecting M points from the Leech lattice (scaled by some factor) in the nearly-optimal shaping region $\mathcal{T}_n(t_n^*)$. Directly shaping M Leech lattice points is challenging and a look-up table may consume unnecessary computation and storage resources due to exponential increase of the cardinality M with β . To address this issue, we design an energy-efficient multidimensional constellation, called *optimally-shaped Leech constellation* (OSLC), based on the aforementioned lattice construction in Eqs. (18) and (19) and the idea of *coarsely shaping and finely coding*, where the constellation shaping function is assigned to a sublattice of the coding lattice (i.e., Λ_{24}).

For better readability, we illustrate the basic idea of coarsely shaping and finely coding with a two-dimensional example in Fig. 1. Suppose that it is required to select M D_2 points with the boundary that forms a given truncated cube. Let us represent D_2 in a construction-A form

$$D_2 = 2\mathbb{Z}^2 + C_2, \quad (20)$$

where the set $C_2 = \{\mathbf{0}^2, \mathbf{1}^2\}$. Naturally, an alternative method is first selecting $M/2$ $2\mathbb{Z}^2$ points from the desired truncated cube (see blue small circles in Fig. 1) and then translating those points by the vector $\mathbf{1}^2$ (see magenta small diamonds in Fig. 1). It can be seen that all points are selected from D_2 lattice which determines the minimum Euclidean distance, say finely coding, and simultaneously the overall boundary almost maintain a desired shape enclosing $M/2$ $2\mathbb{Z}^2$ points, say coarsely shaping.

1) *Constellation Construction*: Motivated by the above idea and the construction-A expression (18) of the Leech half-lattice H_{24} , the boundary of the 24-dimensional constellation \mathcal{X} to be designed can be coarsely controlled by restricting the component D_{24} points in a prescribed geometrical region, which is exactly $\mathcal{T}_{24}(t_{24}^*)$ for our considered OIC under dual intensity constraints. Based on Theorem 2, we may replace the optimal parameter t_{24}^* by $24\alpha + 1/\mu^*$. In the following, the construction of OSLCs are presented in details.

As defined before, the normalized bit rate $\beta = \frac{1}{24} \log_2 M$ for a 24-dimensional constellation \mathcal{X} . Note that there are 2^{13} elements in the coset $[\Lambda_{24}/4D_{24}] = 2G_{24} \cup (2G_{24} + \xi)$.

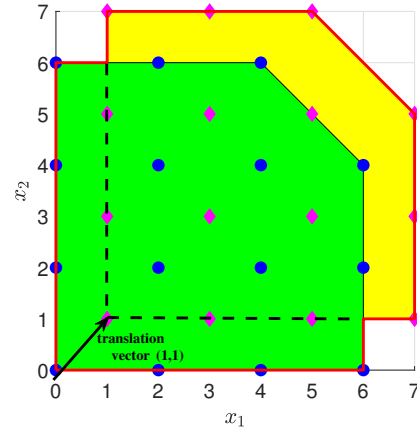


Fig. 1: Coarsely shaping and finely coding for selecting D_2 points from a truncated cube.

Let the constants $k_s = 24\beta - 13$ and $M_s = 2^{k_s}$. Now the constellation shaping problem is converted into how to select M_s D_{24} points in a scaled truncated cube. Define the constant A as the smallest positive number such that

$$|D_{24} \cap A\mathcal{T}_{24}(24\alpha + 1/\mu^*)| \geq M_s,$$

and

$$H^* \triangleq \max_{\mathbf{d} \in D_{24} \cap A\mathcal{T}_{24}(24\alpha + 1/\mu^*)} \|\mathbf{d}\|_{+\infty}, \quad (21a)$$

$$2L^* \triangleq \max_{\mathbf{d} \in D_{24} \cap A\mathcal{T}_{24}(24\alpha + 1/\mu^*)} \|\mathbf{d}\|_1. \quad (21b)$$

Hence, the required shaping set is exactly $\mathcal{D}_{24}(H^*, 2L^*, M_s)$, and fortunately, the aforementioned FDSM algorithm in [19] can be used to map the binary messages onto this set.

Analogue to the above two-dimensional example, we construct the *optimally-shaped Leech constellation* \mathcal{L}_{24} via translating the shaping set $\mathcal{D}_{24}(H^*, 2L^*, M_s)$ by all elements in the coset $[\Lambda_{24}/4D_{24}] = 2G_{24} \cup (2G_{24} + \xi)$, and therefore is expressed as

$$\mathcal{L}_{24} = 2\mathcal{H}_{24} \cup (2\mathcal{H}_{24} + \tilde{\xi}), \quad (22)$$

where the set $\mathcal{H}_{24} \triangleq \mathcal{D}_{24}(H^*, 2L^*, M_s) + G_{24}$ the coset representative $\tilde{\xi}$ satisfies

$$\tilde{\xi} = \begin{cases} (5, 1^{23}) & , 2h_1 \bmod 8 < 3, \\ (-3, 1^{23}) & , 2h_1 \bmod 8 > 3, \end{cases} \quad (23)$$

for less consumed average optical power, and h_1 is the first coordinate of $\mathbf{h} \in \mathcal{H}_{24}$. It can be easily verified that, after the above vector translation, so-constructed constellation still lies in the nonnegative orthant and has a cardinality of M .

To satisfy the intensity constraints in Eq. (2), the constellation needs to be scaled. Note that the average optical power of the OSLC is

$$\begin{aligned} & \frac{1}{24M} \sum_{\mathbf{x} \in \mathcal{L}_{24}} \|\mathbf{x}\|_1 \\ &= \frac{1}{24M} \sum_{\mathbf{x} \in \mathcal{H}_{24}} \|\mathbf{x}\|_1 + \|\mathbf{x} + \tilde{\xi}\|_1 \end{aligned}$$

$$\begin{aligned}
&= \frac{1}{24M} \sum_{\substack{\mathbf{d} \in \mathcal{D}_{24}(H^*, 2L^*, M_s) \\ \mathbf{g} \in G_{24}}} \|\mathbf{4d} + 2\mathbf{g}\|_1 + \|\mathbf{4d} + 2\mathbf{g} + \tilde{\boldsymbol{\xi}}\|_1 \\
&= 1 + \frac{1}{2 \times 24M_s} \sum_{\mathbf{d} \in \mathcal{D}_{24}(H^*, 2L^*, M_s)} \|\mathbf{4d}\|_1 + \|\mathbf{4d} + \tilde{\boldsymbol{\xi}}\|_1 \quad (24) \\
&\approx 1.5 + \frac{1}{6M_s} \sum_{\mathbf{d} \in \mathcal{D}_{24}(H^*, 2L^*, M_s)} \|\mathbf{d}\|_1, \quad (25)
\end{aligned}$$

where Eq. (24) follows from the fact that the averaged sum (over all channel uses) of a linear code is 0.5, and Eq. (25) holds because the average sum of the coset representatives is approximately equal to 0.5.

The peak optical power of OSLC is

$$\begin{aligned}
\max_{\mathbf{x} \in \mathcal{L}_{24}} \|\mathbf{x}\|_\infty &= \max_{\mathbf{d} \in \mathcal{D}_{24}(H^*, 2L^*, M_s)} \|\mathbf{4d} + 2\mathbf{g} + \tilde{\boldsymbol{\xi}}\|_\infty \\
&\leq 7 + \max_{\mathbf{d} \in \mathcal{D}_{24}(H^*, 2L^*, M_s)} \|\mathbf{4d}\|_\infty \quad (26) \\
&= 4H^* + 7, \quad (27)
\end{aligned}$$

where Eq. (26) follows from that fact that the maximum element of the point in Golay codes is 1 and that of the coset representatives is 5, and Eq. (27) holds because of Eq. (21a).

Therefore, the scaling factor is

$$\kappa = 1/\max \left\{ 4H^* + 7, \left(1.5 + \frac{1}{6M_s} \sum_{\mathbf{d} \in \mathcal{D}_{24}(H^*, 2L^*, M_s)} \|\mathbf{d}\|_1 \right) / \alpha \right\}, \quad (28)$$

2) *Constellation Mapping*: The procedures that maps a binary sequence \mathbf{b} onto the OSLC point $\mathbf{x} \in \kappa\mathcal{L}_{24}$ are summarized as follows, and also plotted in Fig. 2 for a clear illustration.

- *Step 1: Data partition*. Let $\mathbf{b} \in \{0, 1\}^k$ be a length- k binary sequence, where $k = 24\beta$. Then we divide \mathbf{b} into three parts $\mathbf{b}_s = (b_1, \dots, b_{k_s})$, $\mathbf{b}_g = (b_{k_s+1}, \dots, b_{k-1})$, and b_k respectively.
- *Step 2: Coarsely shaping*. The binary data \mathbf{b}_s is mapped onto the 24-dimensional lattice point $\mathbf{d} = (d_1, \dots, d_{24}) \in \mathcal{D}_{24}(H^*, 2L^*, M_s)$ by the FDSM algorithm [19, Algorithm 2].
- *Step 3: Golay coding*. Input the binary data \mathbf{b}_g into the (24, 12, 8) Golay encoder, and we can obtain the Golay code $\mathbf{g} = (g_1, \dots, g_{24}) \in G_{24}$.
- *Step 4: Coset mapping*. Select the coset representative of $[\Lambda_{24}/2H_{24}]$. If $b_k = 0$, then $\boldsymbol{\lambda} = \mathbf{4d} + 2\mathbf{g}$. Otherwise, $\boldsymbol{\lambda} = \mathbf{4d} + 2\mathbf{g} + \tilde{\boldsymbol{\xi}}$, where $\tilde{\boldsymbol{\xi}}$ is determined by Eq. (23). The desired constellation point is $\mathbf{x} = \kappa\boldsymbol{\lambda}$.

3) *Demodulation Scheme*: With perfect CSI at the receiver, the maximum likelihood (ML) demodulator for the received signal is

$$\hat{\boldsymbol{\lambda}} = \frac{1}{\kappa} \operatorname{argmin}_{\mathbf{x} \in \kappa\mathcal{L}_{24}} \|\mathbf{x} - \mathbf{r}\|_2 = \operatorname{argmin}_{\boldsymbol{\lambda} \in \mathcal{L}_{24}} \|\boldsymbol{\lambda} - \mathbf{y}\|_2, \quad (29)$$

where $\mathbf{y} = \mathbf{r}/\kappa$ is a scaled version of the received signal. However, the ML demodulator is not feasible in practice due to the complexity limitation. In this paper, a bounded-distance decoding algorithm for the Leech lattice Λ_{24} proposed in [31] is adopted in our demodulation scheme. The main idea of such the bounded-distance algorithm is illustrated as follows.

Let us consider the ML decoding problem for the Leech half lattice H_{24} , which does not admit a construction-A expression. We first review the following construction-A expression of E_{24} lattice

$$E_{24} = 2\mathbb{Z}^{24} + G_{24}, \quad (30)$$

with the (24, 12, 8) Golay code as the binary linear code [28]. Note that D_{24} is a sublattice of \mathbb{Z}^{24} that consists of all the points with even sum. By comparing Eqs. (18) and (30), it is easily seen that H_{24} is a sublattice of E_{24} , and the corresponding coset $[E_{24}/H_{24}] = \{\mathbf{0}^{24}, (\mathbf{0}^m, 2, \mathbf{0}^{24-m-1})\}$, where m can be chosen to be any integer number between 0 and 23. If the noise vector is bounded, then the decoding problem for H_{24} with a construction-C structure can be converted into that for E_{24} with a construction-A structure, for which the closest point search is equivalent to soft decoding of the Golay code [28].

Based on the above fact, we can implement the demodulation by fast searching the closest point in the construction-A lattice E_{24} , and then performing bounded-distance decoding in H_{24} and Λ_{24} . The procedures of our demodulation are summarized in the following.

- *Step 1: Closest point search in E_{24}* [28], [32]. Let $\hat{\mathbf{e}} = 2\hat{\mathbf{n}} + \hat{\mathbf{g}}$ be the closest point in E_{24} to the scaled signal \mathbf{y} , where the integer component $\hat{\mathbf{n}}$ and the Golay code component $\hat{\mathbf{g}}$ are determined by the decoding algorithm for construction-A lattices in [28, p. 450] and the soft decoding algorithm for the Golay code [32, Algorithm 2], respectively.
- *Step 2: Bounded-distance decoding in H_{24}* [31]. Initialize the closest H_{24} lattice point $\hat{\mathbf{h}} = \hat{\mathbf{e}}$. If the sum of the integer component $\hat{\mathbf{n}}$ is odd, we first search the smallest index i satisfying

$$i = \operatorname{argmax}_{j \in \{1, 2, \dots, 24\}} |y_j - e_j|, \quad (31)$$

and then let

$$\hat{h}_i = \begin{cases} \hat{e}_i + 2, & \text{if } y_i \geq \hat{e}_i; \\ \hat{e}_i - 2, & \text{if } y_i < \hat{e}_i. \end{cases} \quad (32)$$

- *Step 3: Bounded-distance decoding in Λ_{24}* [31]. Compute Euclidean distances from \mathbf{y} to $2\hat{\mathbf{h}}$, $2\hat{\mathbf{h}} + (-3, \mathbf{1}^{23})$ and $2\hat{\mathbf{h}} + (5, \mathbf{1}^{23})$, and select the closest one as the demodulator output $\hat{\boldsymbol{\lambda}}$.

Note that the constellation demapping of the demodulator output $\hat{\boldsymbol{\lambda}}$ onto the binary sequence is a simple inverse transform of the constellation mapping, and therefore omitted. Instead, the details of whole decoding procedures (including both constellation demodulation and demapping) for the OSLC are given in Algorithm 1.

V. NUMERICAL RESULTS

In this section, we first numerically verify our asymptotic results on the optimal shaping region. Then the simulated error performance of our proposed OSLC scheme and other benchmark schemes are presented.

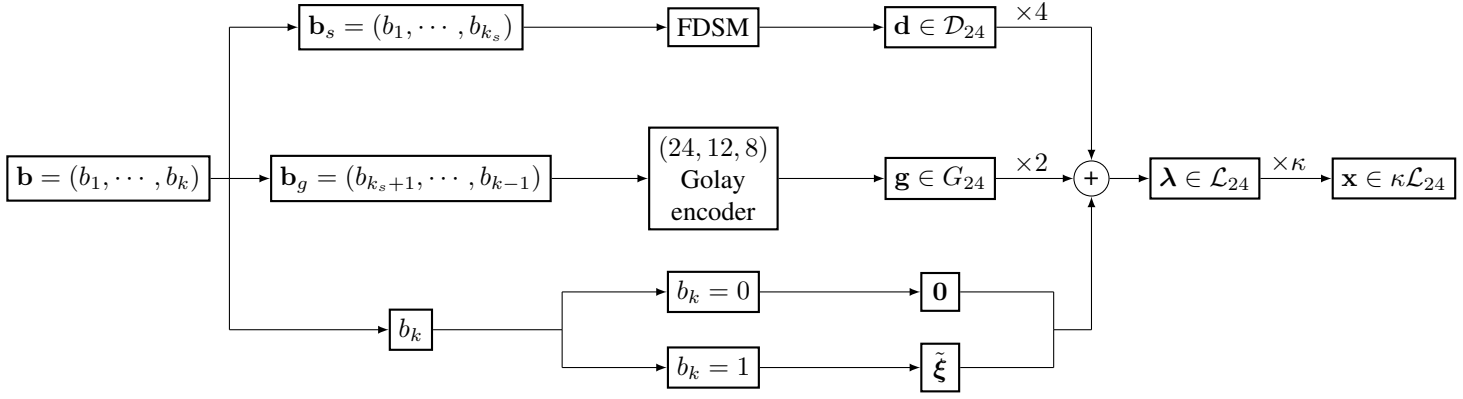


Fig. 2: Diagram of constellation mapping for the OSLC.

Algorithm 1 Decoding of the OSLC.

- 1: **Input:** The received signal $\mathbf{r} = (r_1, \dots, r_k)$.
 - 2: **Output:** The estimated binary sequence $\hat{\mathbf{b}} = (\hat{b}_1, \dots, \hat{b}_k)$.
 - 3: $k_s = k - 13$;
 - 4: $\mathbf{y} = \mathbf{r}/\kappa$;
 - 5: The point $\hat{\mathbf{e}} = 2\hat{\mathbf{n}} + \hat{\mathbf{g}}$ can be obtained by searching the closest point of E_{24} to \mathbf{y} ;
 - 6: Input $\hat{\mathbf{g}}$ to the Golay decoder and the output is $\hat{\mathbf{b}}_g = (\hat{b}_{k_s+1}, \dots, \hat{b}_{k-1})$;
 - 7: $\hat{\mathbf{h}} = \hat{\mathbf{e}}$;
 - 8: **If** $\text{mod}(\|\hat{\mathbf{n}}\|_1, 2) = 1$
 - 9: $i = \arg\max_{j \in \{1, 2, \dots, 24\}} |y_j - e_j|$;
 - 10: **If** $y_i - e_i < 0$
 - 11: $\hat{h}_i = e_i - 2$;
 - 12: **Else**
 - 13: $\hat{h}_i = e_i + 2$;
 - 14: **End**
 - 15: **End**
 - 16: $\hat{\mathbf{d}} = (\hat{\mathbf{h}} - \hat{\mathbf{g}})/2$;
 - 17: Map $\hat{\mathbf{d}}$ onto the binary sequence $\hat{\mathbf{b}}_s = (\hat{b}_1, \dots, \hat{b}_{k_1})$ by the FFT-assisted decomposable shell demapping algorithm in [19, Algorithm 3];
 - 18: $\hat{\lambda}_1 = 2\hat{\mathbf{h}}; \hat{\lambda}_2 = 2\hat{\mathbf{h}} + (-3, 1^{23}); \hat{\lambda}_3 = 2\hat{\mathbf{h}} + (5, 1^{23})$;
 - 19: $l_j = \|\mathbf{y} - \hat{\lambda}_j\|_2, \forall j \in \{1, 2, 3\}$;
 - 20: $m = \arg\min_{j \in \{1, 2, 3\}} l_j$;
 - 21: **If** $m = 1$
 - 22: $\hat{b}_k = 0$;
 - 23: **Else**
 - 24: $\hat{b}_k = 1$;
 - 25: **End**
-

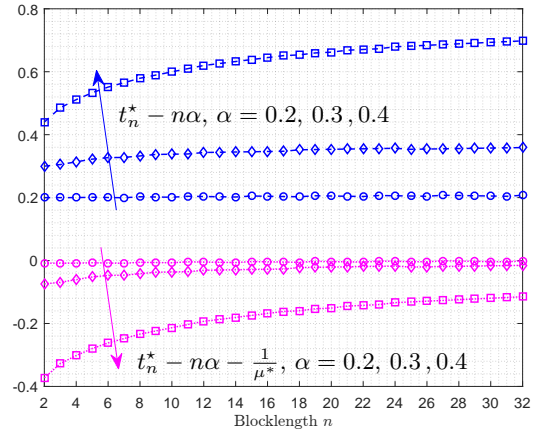


Fig. 3: The approximation error $t_n^* - n\alpha - 1/\mu^*$ versus various blocklengths n and constraint parameters α .

Fig. 4 provides the relationship between the maximum shaping gain $\bar{\gamma}_\alpha(n)$ and the constraint parameter α in various dimensions. It can be seen from Fig. 4 that for any $\alpha \in (0, \frac{1}{2})$, the gap between the ultimate shaping gain and the maximum shaping gain obtained in the 32-dimensional space is no larger than 0.2 dB, which indicates that most of the shaping gain can be obtained at low dimensions.

Based on Theorem 3, we can use the second-order expansion in (13) to approximate the maximum shaping gain in finite dimensions. In Fig. 5, we plot the true maximum shaping gains and the approximated shaping gains versus various dimensions n and different intensity constraint parameters α . The results show that the true maximum shaping gain can be effectively approximated by second-order approximation. When $n \geq 16$, the approximate error is no larger than 0.1 dB.

A. Optimal Shaping Parameter and Maximum Shaping Gain

As a consequence of Theorem 2, we may approximate the shaping parameter t_n^* by $n\alpha + 1/\mu^*$ in the application of lattice codes. In Fig. 3, we plot the absolute approximation error $t_n^* - n\alpha - 1/\mu^*$ for blocklengths n from 2 to 32, which shows a good approximation performance even at very short blocklengths.

B. Error Performance

1) *AWGN Channel:* In this subsection, we present the symbol error rate (SER) curves of the proposed OSLC and two benchmark schemes over AWGN channels. One benchmark is the cubic constellation, which is the n -times Cartesian product of a size- 2^β ASK constellation. Another is the D_n -based TCC given in [19].

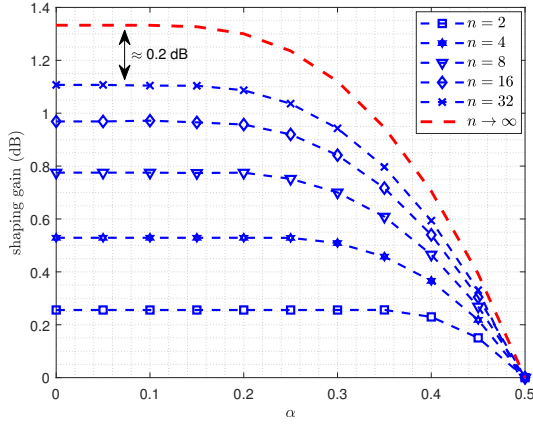


Fig. 4: The relationship between the maximum shaping gain $\bar{\gamma}_\alpha(n)$ and the constraint parameter α with different dimensions.

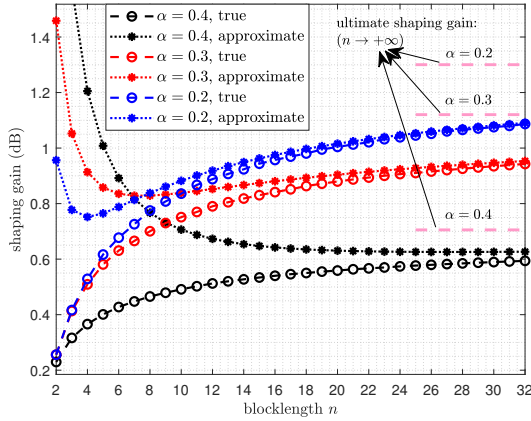


Fig. 5: True shaping gain and the second-order approximation with different constraint parameters.

Fig. 6 plots the SER curves of the cubic constellation, the TCC, and the proposed OSLC with $\alpha = 0.2$ and the normalized bit rate β varying from 2 bpcu to 5 bpcu, while Fig. 7 plots those curves in the case of $\alpha = 0.3$. It can be seen from Fig. 6(a) and Fig. 7(a) that the TCC outperforms the OSLC at $\beta = 2$ and the error performance of these two schemes is nearly the same at $\beta = 3$. The main reasons come from two aspect: 1) by using the coarsely shaping and fine coding strategy, only a small part of the binary sequence is mapped onto D_{24} points when β is small, which simultaneously makes the final shaping region far less like the optimal shaping region and break the structure of the Leech lattice; 2) A bounded-distance Leech lattice decoding method is used to demodulated the OSLC that is a subset of the Leech lattice. In Fig. 6(b) and Fig. 7(b), we observe that our proposed OSLC significantly outperforms the TCC and the cubic constellation at $\beta = 4$ or $\beta = 5$. In the case of $\alpha = 0.2$ and $\beta = 4$ or $\beta = 5$, the OSLC has SNR gains of 2.3 dB and 0.6 dB at a target SER 10^{-5} , as compared to the TCC and the cubic constellation, respectively, while the corresponding SNR gains of 2.1 dB and 0.5 dB

can be observed when $\alpha = 0.3$. The reduction in the SNR gain is primarily stemmed from the fact that the maximum shaping gain at any dimension is monotonically decreasing as the quantity α increases to $\frac{1}{2}$.

Herein, we also evaluate the gap between our proposed OSLC and the Shannon limit. Unlike the radio-frequency channel, there is no closed-form formula to calculate the channel capacity of the OIC, and hence, we use the upper and lower bounds on the channel capacity given in [7], [8] and plot them in the form of semitransparent wide strips. From Fig. 6(b), it can be seen that at a target SER 10^{-5} the gap between our scheme and the Shannon limit is 2.1 – 2.7 dB when $\alpha = 0.2$ and $\beta = 4$, and the gap is 2.1 – 2.4 dB when $\beta = 5$. From Fig. 7(b), the gaps are about 2.1 – 2.6 dB and 2.1 – 2.4 dB in the case of $\alpha = 0.3$ and $\beta = 4$ and that of $\alpha = 0.3$ and $\beta = 5$, respectively.

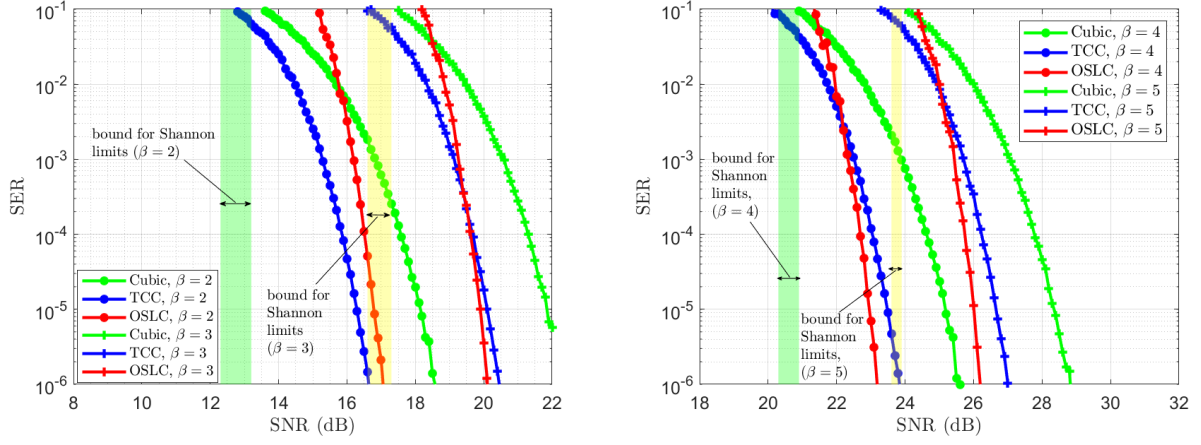
2) *Indoor VLC Scenario:* We particularly provide a glimpse of the error performance of our proposed scheme in an indoor VLC scenario, where a $4\text{m} \times 4\text{m} \times 3\text{m}$ room with 4 LED lamps is considered. We assume that the LED lamps are installed on the ceiling and equipped with 7×7 LED array, and the receiver PD is located on the plane at height of 0.6m . Other configuration parameters of the LED transmitter and the PD receiver is list in Tables I and II. From the result in [33], such the MISO VLC channel with a same LED configuration can be equivalent to a scalar VLC channel. We plot the simulated SER for the considered indoor VLC scenario in Fig. 8. It can be seen that, the received SNRs are about 25 – 26 dB. From simulation results for the AWGN channel, high data rates such as $\beta = 5$ can be realized at those high SNRs. Table III lists the average SER of our proposed scheme and the benchmarks with the normalized bit rate $\beta = 5$ for the considered indoor channel, where the receiver PD is randomly located at (X, Y) and coordinates X and Y are independently and uniformly distributed on the interval $[-4, 4]$. Numerical results also verify the performance advantage of our schemes than others.

TABLE I: Transmitter Parameters

LED lamp coordinates	$[\pm 1.6, \pm 1.6, 3]$
Low drive current	400 [mA]
High drive current	600 [mA]
Semi-angle at half power	60°
LED interval	1 [cm]
O/E conversion efficiency of LED	0.5 [W/A]

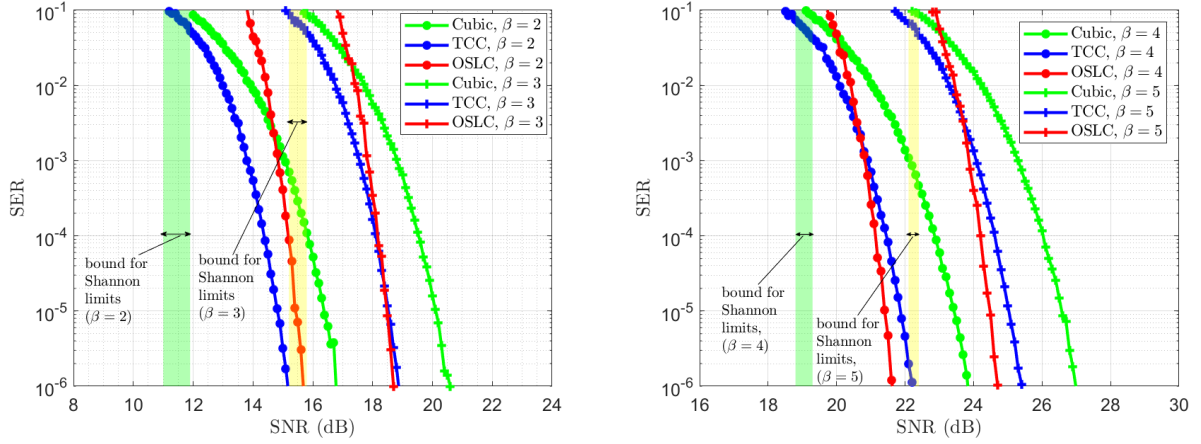
VI. CONCLUSION

In this paper, for the indoor VLC channel with a peak- and an average-intensity constraints, we proposed a geometrically-shaped constellation design based on Leech lattice, which mainly consists of the asymptotics of the optimal constellation shaping region and the coarsely shaping and finely coding strategy of constellation construction. The proposed optimally-shaped Leech constellation incorporates the nearly-maximum shaping gain and a larger coding gain, and has shown superiority in performance compared to the benchmark schemes.



(a) The SER curves of the OSLC scheme and the benchmarks with $\alpha = 0.2$ when $\beta = 2$ bpcu and 3 bpcu. (b) The SER curves of the OSLC scheme and the benchmarks with $\alpha = 0.2$ when $\beta = 4$ bpcu and 5 bpcu.

Fig. 6: The SER curves of the OSLC scheme and the benchmarks with $\alpha = 0.2$.



(a) The SER curves of the OSLC scheme and the benchmarks with $\alpha = 0.3$ when $\beta = 2$ bpcu and 3 bpcu. (b) The SER curves of the OSLC scheme and the benchmarks with $\alpha = 0.3$ when $\beta = 4$ bpcu and 5 bpcu.

Fig. 7: The SER curves of the OSLC scheme and the benchmarks with $\alpha = 0.3$.

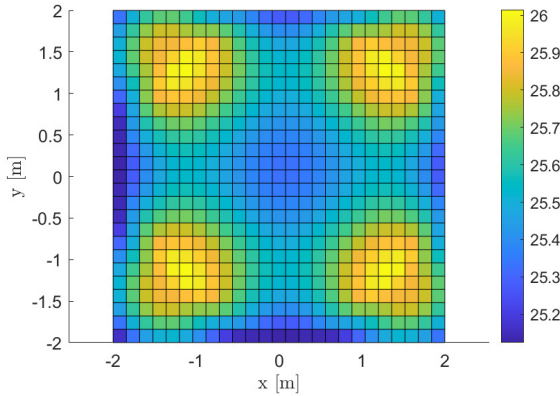


Fig. 8: The simulation of SNR for the 4m×4m×3m room.

TABLE II: Receiver Parameters

Physical area of PD	1 [cm ²]
Gain of optical filter	1
Refractive index of the lens at PD	1.5
Responsivity of PD	0.4 [A/W]
FOV (field of view)	60°
System bandwidth	10 [MHz]
Noise bandwidth factor	0.562
Background current	100 [μA]

ACKNOWLEDGEMENT

This work is supported by the National Natural Science Foundation of China (NSFC) under Grant (62071489).

TABLE III: Average SER for the indoor VLC system.

Average SER \ Parameter α	0.2	0.3
Scheme		
Cubic constellation	0.0168	4.621×10^{-4}
TCC	0.0013	1.065×10^{-6}
OSLC	7.501×10^{-4}	$\ll 10^{-6}$

APPENDIX A TRUNCATED CUBES

As defined in [34], the n -dimensional *truncated cube* $\mathcal{T}_n(t)$ with the largest coordinate t , $t \in [0, n]$, is the intersection of a unit n -cube with an n -simplex as follows

$$\mathcal{T}_n(t) \triangleq \left\{ \mathbf{x} \in [0, 1]^n : \sum_{i=1}^n x_i \leq t \right\} \quad (33)$$

The volume and average first moment of $\mathcal{T}_n(t)$ are given by

$$V_n(t) = \frac{1}{n!} \sum_{k=0}^n \binom{n}{k} (-1)^k (t-k)^n \mathbf{1}_{\mathbb{R}_+}(t-k) \quad (34)$$

and

$$P_n(t) = \frac{1}{n} \left(t - \frac{\sum_{k=0}^n \binom{n}{k} (-1)^k (t-k)^{n+1} \mathbf{1}_{\mathbb{R}_+}(t-k)}{V_n(t) \cdot (n+1)!} \right), \quad (35)$$

respectively, where the indicator function $\mathbf{1}_{\mathbb{R}_+}(x)$ equals one if $x \geq 0$ and otherwise zero [19].

APPENDIX B LARGE DEVIATION OF SUM OF INDEPENDENT RANDOM VARIABLES UNIFORMLY DISTRIBUTED ON $[0, 1]$

Let the random variable U be uniformly distributed on $[0, 1]$. For $s > 0$, the moment-generating function of U is

$$M(s) \triangleq \mathbb{E}[\exp(sU)] = \frac{\exp(s) - 1}{s},$$

and we define

$$K(s) \triangleq \frac{M'(s)}{M(s)} = \frac{\exp(s)}{\exp(s) - 1} - \frac{1}{s}.$$

It is clear that $K(s)$ is monotone increasing and satisfies $K(0^+) = \frac{1}{2}$ and $K(+\infty) = 1$. Then, we let s_x denote the unique solution to the equation

$$K(s_x) = x, \quad (36)$$

where $x \in [\frac{1}{2}, 1]$. Specially, an immediate consequence of (11) is

$$\mu^* = s_{1-\alpha}. \quad (37)$$

Clearly, the solution s_x increases with x . Then, for $x \in [\frac{1}{2}, 1]$, we define

$$L(x) \triangleq \log(M(s_x)) - x s_x,$$

and

$$D(x) \triangleq s_x \sqrt{K'(s_x)} = \sqrt{\frac{-s_x^2 \cdot \exp(s_x)}{(\exp(s_x) - 1)^2}} + 1.$$

It can be easily verified both $L(x)$ and $D(x)$ are smooth. Then, by computing high-order derivatives of $D(x)$, we can show that $D(x)$ is bounded and non-decreasing with x . Also, we note that

$$L'(x) = \left(\frac{M'(s_x)}{M(s_x)} - x \right) \cdot \frac{ds_x}{dx} - s_x \quad (38)$$

$$= (K(s_x) - x) \cdot \frac{ds_x}{dx} - s_x \quad (39)$$

$$= -s_x. \quad (40)$$

Since s_x is increasing as x increases, the function $L(x)$ is concave and thus satisfies

$$L(x) \leq L(1 - \tau) - s_{1-\tau}(x - (1 - \tau)). \quad (41)$$

for any x and τ in $[\frac{1}{2}, 1]$.

Denote the tail probability of the sample mean $\bar{U}_n = \frac{1}{n} \sum_{i=1}^n U_i$ by $G_n(x) = \mathbb{P}\{\bar{U}_n \geq x\}$. Based on Theorem 1 in [35], the sequence of functions

$$G_n(x) = \frac{\exp(nL(x))}{\sqrt{2\pi n D(x)}} (1 + o(1)) \quad (42)$$

as $n \rightarrow \infty$ uniformly in x in the closed interval $[\frac{1}{2} + \epsilon, 1 - \epsilon]$, where ϵ is an arbitrarily positive constant.

APPENDIX C PROOF OF THEOREM 2

The average first moment of $\mathcal{T}_n(n\tau)$ can be alternatively expressed by the conditional expectation of the Irwin-Hall distribution as follows

$$P_n(n\tau) = \frac{1}{n} \sum_{i=1}^n \mathbb{E} \left[U_i \mid \sum_{i=1}^n U_i \leq n\tau \right] \quad (43)$$

$$= \mathbb{E}[\bar{U}_n \mid \bar{U}_n \leq \tau] \quad (44)$$

$$= 1 - \mathbb{E}[\bar{U}_n \mid \bar{U}_n \geq 1 - \tau]. \quad (45)$$

Remind that the tail probability $G_n(x) = \mathbb{P}\{\bar{U}_n \geq x\}$. Then, it is straightforward that

$$P_n(n\tau) = 1 + \frac{\int_{1-\tau}^1 x dG_n}{G_n(1-\tau)} \quad (46)$$

$$= \tau - \int_{1-\tau}^1 \frac{G_n(x)}{G_n(1-\tau)} dx. \quad (47)$$

The first-moment condition (8) immediately shows that

$$\alpha = \tau_n^* - \int_{1-\tau_n^*}^1 \frac{G_n(x)}{G_n(1-\tau_n^*)} dx. \quad (48)$$

It is clear that $\tau_n^* \geq \alpha$ for any n . Next, we will prove that

$$\lim_{n \rightarrow \infty} n(\tau_n^* - \alpha) = \frac{1}{s_{1-\alpha}}. \quad (49)$$

Note that $\tau \geq \alpha$ and $P_n(1) = \frac{1}{2}$. For any $\tau \in (0, 1)$, there exists a positive (and possibly arbitrarily small) constant ϵ such that $1 - \tau + 2\epsilon \leq 1$. Then we note that

$$0 \leq \int_{1-\tau}^1 \frac{G_n(x)}{G_n(1-\tau)} dx \leq 2\epsilon + \int_{1-\tau+\epsilon}^{1-\epsilon} \frac{G_n(x)}{G_n(1-\tau)} dx. \quad (50)$$

Due to the uniform convergence of $G_n(x)$, we can rewrite

$$\begin{aligned}
& \int_{1-\tau+\epsilon}^{1-\epsilon} G_n(x) dx \\
&= \int_{1-\tau+\epsilon}^{1-\epsilon} \frac{\exp(nL(x))}{\sqrt{2\pi n D(x)}} (1+o(1)) dx \\
&\leq \int_{1-\tau+\epsilon}^{1-\epsilon} \frac{\exp(n(L(1-\tau) - s_{1-\tau}(x - (1-\tau))))}{\sqrt{2\pi n D(1-\tau)}} (1+o(1)) dx \\
&\leq \frac{1}{s_{1-\tau}} G_n(1-\tau) \left(\frac{1}{n} + o\left(\frac{1}{n}\right) \right)
\end{aligned} \tag{51}$$

Immediately, we have $\tau_n^* = \alpha + o(1)$. Note that

$$n(\tau_n^* - \alpha) \tag{52}$$

$$\begin{aligned}
&= n \int_{1-\tau_n^*}^1 \frac{G_n(x)}{G_n(1-\tau_n^*)} dx \\
&\leq n \left(\int_{1-\tau_n^*}^{1-\epsilon} \frac{G_n(x)}{G_n(1-\tau_n^*)} dx + \epsilon \frac{G_n(1-\epsilon)}{G_n(1-\tau_n^*)} \right)
\end{aligned} \tag{53}$$

$$= \frac{1}{s_{1-\alpha}} + o(1) \tag{54}$$

On the one hand, for any finite $k \in \mathbb{N}$, we have

$$n \int_{1-\tau_n^*}^1 \frac{G_n(x)}{G_n(1-\tau_n^*)} dx \tag{55}$$

$$\begin{aligned}
&\geq n \int_{1-\tau_n^*}^{1-\tau_n^*+\frac{k}{n}} \frac{G_n(x)}{G_n(1-\tau_n^*)} dx \\
&= n \int_0^{\frac{k}{n}} \exp(-ns_{1-\tau_n^*}x) dx \cdot (1+o(1))
\end{aligned} \tag{56}$$

$$= \frac{1 - \exp(-ks_{1-\tau_n^*})}{s_{1-\alpha}} (1+o(1)). \tag{57}$$

(37), (54) and (57) complete the proof of Theorem 2.

APPENDIX D PROOF OF THEOREM 3

It should be noted that:

$$\begin{aligned}
&\log(\bar{\gamma}_\alpha(n)) + \log(2\alpha) \\
&= \frac{1}{n} \log(\text{vol}(\mathcal{T}_n(t_n^*))) \\
&= \frac{1}{n} \log(G_n(1-\tau_n^*)) \\
&= \frac{1}{n} \log\left(\frac{\exp(nL(1-\tau_n^*))}{\sqrt{2\pi n D(1-\tau_n^*)}} (1+o(1))\right) \\
&= L\left(1-\alpha - \frac{1}{\mu^*} \frac{1}{n} + o\left(\frac{1}{n}\right)\right) + o\left(\frac{1}{n}\right) \\
&\quad - \frac{1}{n} \log\left(\sqrt{2\pi n D}\left(1-\alpha - \frac{1}{\mu^*} \frac{1}{n} + o\left(\frac{1}{n}\right)\right)\right)
\end{aligned} \tag{58}$$

$$\begin{aligned}
&= L(1-\alpha) - \frac{\log(2\pi n)}{2n} + \frac{1}{n} (1 - \log(D(1-\alpha))) + o\left(\frac{1}{n}\right) \\
&= h_{\max} - \frac{\log(n)}{2n} + o\left(\frac{1}{n}\right)
\end{aligned} \tag{60}$$

$$+ \frac{1}{n} \left(1 - \frac{1}{2} \log\left(2\pi\left(-\mu^* + 2\alpha\mu^* + (\mu^*)^2\alpha(1-\alpha)\right)\right) \right) \tag{61}$$

$$= h_{\max}(\alpha) - \log(2\alpha) - \frac{\log(n)}{2n} + \frac{\omega_\alpha}{n} + o\left(\frac{1}{n}\right) \tag{62}$$

where Eq. (58) is obtained by Eq. (42), Eq. (59) is derived from Theorem 2 Eq. (60) is calculated by

$$\begin{aligned}
&L\left(1-\alpha - \frac{1}{\mu^*} \frac{1}{n} + o\left(\frac{1}{n}\right)\right) \\
&= L(1-\alpha) + L'(1-\alpha) \left(-\frac{1}{\mu^*} \frac{1}{n} + o\left(\frac{1}{n}\right)\right) + o\left(\frac{1}{n}\right) \\
&= L(1-\alpha) - s_{1-\alpha} \left(-\frac{1}{\mu^*} \frac{1}{n} + o\left(\frac{1}{n}\right)\right) + o\left(\frac{1}{n}\right) \\
&= L(1-\alpha) + \frac{1}{n} + o\left(\frac{1}{n}\right),
\end{aligned} \tag{63}$$

and $D\left(1-\alpha - \frac{1}{\mu^*} \frac{1}{n} + o\left(\frac{1}{n}\right)\right) = D(1-\alpha) + o(1)$, and Eq. (61) can be obtained by substitute the value into $L(1-\alpha)$ and $D(1-\alpha)$.

APPENDIX E PROOF OF PROPOSITION 4

Due to $\tau_n^* \geq \alpha$, for a given constant $\alpha > 0$ and sufficiently large n , $t_n^* \gg 1$. Therefore, the marginal cumulative distribution can be expressed as

$$\begin{aligned}
F_{X_1,n}(x) &= \mathbb{P}\{X_1 \leq x\} \\
&= \frac{\int_0^x V_{n-1}(t_n^* - y) dy}{V_n(t_n^*)}, \quad x \in [0, 1].
\end{aligned} \tag{64}$$

whose derivative is the desired PDF and satisfies

$$\begin{aligned}
&f_{X_1,n}(x) \\
&= \frac{V_{n-1}(t_n^* - x)}{V_n(t_n^*)}
\end{aligned} \tag{65}$$

$$\begin{aligned}
&= \frac{G_{n-1}\left(1 + \frac{x}{n-1} - \tau_n^* \frac{n}{n-1}\right)}{G_n(1-\tau_n^*)} \\
&= \frac{\sqrt{n}}{\sqrt{n-1}} \frac{\exp\left((n-1)L\left(1 + \frac{x}{n-1} - \tau_n^* \frac{n}{n-1}\right)\right)}{\exp(nL(1-\tau_n^*))}
\end{aligned} \tag{66}$$

$$\begin{aligned}
&\cdot \frac{D(1-\tau_n^*)}{D\left(1 + \frac{x}{n-1} - \tau_n^* \frac{n}{n-1}\right)} (1+o(1)) \\
&= \exp(-L(1-\tau_n^*) + L'(1-\tau_n^*)(x - \tau_n^*)) (1+o(1))
\end{aligned} \tag{67}$$

$$= \exp(-L(1-\alpha) - s_{1-\alpha}(x - \alpha)) (1+o(1)) \tag{68}$$

$$= \exp(-L(1-\alpha) - s_{1-\alpha}(x - \alpha)) (1+o(1)) \tag{69}$$

where (68) follows from the continuity of $D(x)$.

Hence, we have

$$\begin{aligned}
f_\infty(x) &= \exp(-L(1-\alpha) - s_{1-\alpha}(x - \alpha)) \\
&= \frac{1}{M(\mu^*)} \exp((1-\alpha)\mu^* - \mu^*(x - \alpha))
\end{aligned} \tag{70}$$

$$= \frac{\exp(\mu^*)}{M(\mu^*)} \exp(-\mu^*x) \tag{71}$$

$$= \frac{\mu^*}{1 - \exp(-\mu^*)} \exp(-\mu^*x). \tag{72}$$

REFERENCES

- [1] M. S. A. Mossaad, S. Hranilovic, and L. Lampe, "Visible light communications using OFDM and multiple LEDs," *IEEE Transactions on Communications*, vol. 63, no. 11, pp. 4304–4313, 2015.
- [2] Y.-Y. Zhang, "Intrinsic robustness of MISO visible light communications: Partial CSIT can be as useful as perfect one," *IEEE Transactions on Communications*, vol. 67, no. 2, pp. 1297–1312, 2019.
- [3] Z. Zhang and A. Chaaban, "Capacity bounds for the two-user IM/DD interference channel," *IEEE Transactions on Communications*, vol. 70, no. 9, pp. 5960–5974, 2022.
- [4] J. M. Kahn and J. R. Barry, "Wireless infrared communications," *Proc. IEEE*, vol. 85, pp. 265–298, Feb. 1997.
- [5] S. Hranilovic, *Wireless Optical Communication Systems*. New York, NY, USA: Springer Verlag, 2005.
- [6] A. Chaaban, Z. Rezki, and M.-S. Alouini, "On the capacity of intensity-modulation direct-detection Gaussian optical wireless communication channels: A tutorial," *IEEE Communications Surveys & Tutorials*, vol. 24, no. 1, pp. 455–491, 2022.
- [7] A. Lapidith, S. M. Moser, and M. A. Wigger, "On the capacity of free-space optical intensity channels," *IEEE Transactions on Information Theory*, vol. 55, no. 10, pp. 4449–4461, 2009.
- [8] A. A. Farid and S. Hranilovic, "Channel capacity and non-uniform signalling for free-space optical intensity channels," *IEEE Journal on Selected Areas in Communications*, vol. 27, pp. 1553–1563, Dec. 2009.
- [9] S. M. Moser, L. Wang, and M. Wigger, "Capacity results on multiple-input single-output wireless optical channels," *IEEE Transactions on Information Theory*, vol. 64, no. 11, pp. 6954–6966, 2018.
- [10] L. Li, S. M. Moser, L. Wang, and M. Wigger, "On the capacity of MIMO optical wireless channels," *IEEE Transactions on Information Theory*, vol. 66, no. 9, pp. 5660–5682, 2020.
- [11] R.-H. Chen, L. Li, J. Zhang, W. Zhang, and J. Zhou, "On the capacity of MISO optical intensity channels with per-antenna intensity constraints," *IEEE Transactions on Information Theory*, vol. 68, no. 6, pp. 3920–3941, 2022.
- [12] H. Marshoud, P. C. Sofotasios, S. Muhaidat, G. K. Karagiannidis, and B. S. Sharif, "On the performance of visible light communication systems with non-orthogonal multiple access," *IEEE Transactions on Wireless Communications*, vol. 16, no. 10, pp. 6350–6364, 2017.
- [13] U. Thummaluri, A. Kumar, and L. Natarajan, "MIMO codes for uniform illumination across space and time in VLC with dimming control," *IEEE Photonics Journal*, vol. 11, no. 3, pp. 1–21, 2019.
- [14] Y.-Y. Zhang, H.-Y. Yu, and J.-K. Zhang, "Block precoding for peak-limited MISO broadcast VLC: Constellation-optimal structure and addition-unique designs," *IEEE Journal on Selected Areas in Communications*, vol. 36, no. 1, pp. 78–90, 2018.
- [15] Y.-Y. Zhang, H.-Y. Yu, J.-K. Zhang, Y.-J. Zhu, and T. Wang, "Energy-efficient space-time modulation for indoor MISO visible light communications," *Optics Letters*, vol. 41, pp. 329–332, Jan 2016.
- [16] J. Karout, G. Kramer, F. R. Kschischang, and E. Agrell, "A two-dimensional signal space for intensity-modulated channels," *IEEE Communications Letters*, vol. 16, no. 9, pp. 1361–1364, 2012.
- [17] D. Zhang and S. Hranilovic, "Bandlimited optical intensity modulation under average and peak power constraints," *IEEE Transactions on Communications*, vol. 64, no. 9, pp. 3820–3830, 2016.
- [18] G. D. Forney, Jr. and G. Ungerboeck, "Modulation and coding for linear Gaussian channels," *IEEE Transactions on Information Theory*, vol. 44, pp. 2384–2415, May 1998.
- [19] R.-H. Chen, J. Zhang, and Y.-Y. Zhang, "FFT-assisted coded modem for intensity-modulated signals under peak and average power constraints," *IEEE Transactions on Communications*, vol. 68, no. 1, pp. 274–288, 2020.
- [20] G. R. Lang and F. M. Longstaff, "A Leech lattice modem," *IEEE Journal on Selected Areas in Communications*, vol. 7, pp. 968–973, Aug. 2002.
- [21] R. Zamir, *Lattice Coding for Signals and Networks*. Cambridge University Press, 2004.
- [22] F. Kschischang and S. Pasupathy, "Optimal shaping properties of the truncated polydisc," *IEEE Transactions on Information Theory*, vol. 40, no. 3, pp. 892–903, 1994.
- [23] T. Komine and M. Nakagawa, "Fundamental analysis for visible-light communication system using LED lights," *IEEE Transactions on Consumer Electronics*, vol. 50, no. 1, pp. 100–107, 2004.
- [24] G. D. Forney, Jr. and L.-F. Wei, "Multidimensional constellations—Part I: Introduction, figures of merit, and generalized cross constellations," *IEEE Journal on Selected Areas in Communications*, vol. 7, pp. 877–892, Aug. 1989.
- [25] D.-S. Shiu and J. Kahn, "Shaping and nonequiprobable signaling for intensity-modulated signals," *IEEE Transactions on Information Theory*, vol. 45, no. 7, pp. 2661–2668, 1999.
- [26] J. Leech, "Notes on sphere packing," vol. 19, pp. 251–267, 1967.
- [27] H. Cohn, A. Kumar, S. D. Miller, D. Radchenko, and M. Viazovska, "The sphere packing problem in dimension 24," *Annals of Mathematics*, vol. 185, no. 3, pp. 1017–1033, 2017.
- [28] J. Conway and N. J. A. Sloane, *Sphere Packings, Lattices and Groups*. New York, NY, USA: Springer Verlag, 3rd ed., 1999.
- [29] G. Forney, "Coset codes. I. introduction and geometrical classification," *IEEE Transactions on Information Theory*, vol. 34, no. 5, pp. 1123–1151, 1988.
- [30] O. Amrani, Y. Be'ery, A. Vardy, F.-W. Sun, and H. van Tilborg, "The Leech lattice and the Golay code: bounded-distance decoding and multilevel constructions," *IEEE Transactions on Information Theory*, vol. 40, no. 4, pp. 1030–1043, 1994.
- [31] G. Forney, "A bounded-distance decoding algorithm for the Leech lattice, with generalizations," *IEEE Transactions on Information Theory*, vol. 35, no. 4, pp. 906–909, 1989.
- [32] R.-H. Chen, Z.-R. Zhu, J. Zhang, J. Qu, and Y. Zuo, "Optimal hexagonal constellations based on a two-dimensional signal space for peak-limited intensity-modulated channels," *IEEE Communications Letters*, vol. 23, no. 2, pp. 254–257, 2019.
- [33] L. Li, R.-H. Chen, Y.-Y. Zhang, J.-N. Guo, and J. Zhang, "Space-time constellation for MU-MISO dimmable visible light communications," *IEEE Communications Letters*, vol. 25, no. 7, pp. 2329–2332, 2021.
- [34] A. K. Khandani and P. Kabal, "Shaping multidimensional signal spaces—Part II: Shell-addressed constellations," *IEEE Transactions on Information Theory*, vol. 39, pp. 1809–1819, Nov. 1993.
- [35] V. V. Petrov, "On the probabilities of large deviations for sums of independent random variables," *Theory of Probability & Its Applications*, vol. 10, no. 2, pp. 287–298, 1965.